Astronomy & Astrophysics

Multi-wavelength structure analysis of local cluster galaxies

The WINGS project[*]

A. Psychogyios[1,2], M. Vika[2], V. Charmandaris[1,2,3], S. Bamford[4], G. Fasano[5], B. Häußler[6], A. Moretti[5], B. Poggianti[5], and B. Vulcani[7,5]

[1] Department of Physics, University of Crete, Herakleio, Greece
   e-mail: alpsych@physics.uoc.gr
[2] IAASARS, National Observatory of Athens, 15236 Penteli, Greece
[3] Institute of Astrophysics, Foundation for Research and Technology-Hellas, 71110 Heraklion, Greece
[4] School of Physics & Astronomy, The University of Nottingham, University Park, Nottingham NG7 2RD, UK
[5] INAF, Osservatorio Astronomico di Padova, Vicolo Osservatorio 5, 35122 Padova, Italy
[6] European Southern Observatory, Alonso de Cordova 3107, Vitacura, Casilla 19001, Santiago, Chile
[7] School of Physics, University of Melbourne, VIC 3010, Australia

ABSTRACT

We present a multi-wavelength analysis of the galaxies in nine clusters selected from the WINGS dataset, examining how galaxy structure varies as a function of wavelength and environment using the state of the art software GALAPAGOS-2. We simultaneously fit single-Sérsic functions on three optical (u, B and V) and two near-infrared (J and K) bands thus creating a wavelength-dependent model of each galaxy. We measure the magnitudes, effective radius (R_e), the Sérsic index (n), axis ratio, and position angle in each band. The sample contains 790 cluster members (located close to the cluster centre $<0.64 \times R_{200}$) and 254 non-member galaxies that we further separate based on their morphology into ellipticals, lenticulars, and spirals. We find that the Sérsic index of all galaxies inside clusters remains nearly constant with wavelength while R_e decreases as wavelength increases for all morphological types. We do not observe a significant variation on n and R_e as a function of projected local density and distance from the clusters centre. Comparing the n and R_e of bright cluster galaxies with a subsample of non-member galaxies we find that bright cluster galaxies are more concentrated (display high n values) and are more compact (low R_e). Moreover, the light profile ($\mathcal{N}$) and size ($\mathcal{R}$) of bright cluster galaxies does not change as a function of wavelength in the same manner as non-member galaxies.

Key words. galaxies: clusters: general – galaxies: structure

1. Introduction

A large fraction of the galaxies in the local Universe have been observed and statistically analysed and it is widely accepted that only a few galaxies are found isolated in the field, while the majority of them are preferentially located in denser environments such as groups or clusters (Schmidt et al. 1997; Robotham et al. 2011). Clusters of galaxies are described as dense peaks in the galaxy distribution across the sky, which were slowly created when the first massive dark matter halos were decoupled from the nearly homogeneous, expanding Universe.These clusters contain hundreds up to thousands of member galaxies.

Observationally, since all galaxies that belong to a cluster are approximately at the same distance from us, we can easily trace their evolution as individual systems as well as how they are affected by the properties of the cluster as a whole. Moreover, since the relative distances between cluster galaxies is rather often comparable to their size, processes such as ram pressure (Gunn & Gott 1972), harassment (Moore et al. 1996, 1998, 1999), tidal forces (Byrd & Valtonen 1990), interaction and merging (Icke 1985; Bekki 1998), as well as starvation and

strangulation of star formation (Larson et al. 1980) speed up galaxy evolution. The study of local galaxy clusters is therefore of paramount importance as they can be used to easily quantify changes in the properties of their members as a function of the baryonic density in the environment, and to place constraints as a reference "zero-point" for comparison with similar studies at higher redshifts.

Even though it was Hubble & Humason (1931) who found that "the predominance of early-types is a conspicuous feature of clusters in general", the systematic study of the properties of galaxy clusters began some decades later when improvements to observing facilities enabled these studies to be done in more detail. One of the first major findings was by Butcher & Oemler (1978) who showed that the fraction of blue galaxies was higher in clusters at $z \gtrsim 0.4$ than in nearby clusters. This result was interpreted as the ageing of spiral galaxies after consuming their gas supply and therefore diminishing their star formation rates.

Dressler (1980) focused on the variation of galaxy properties inside the clusters and found that early-type galaxies are more abundant in the central part of galaxy clusters, a result that is known today as the morphology–density relation. In addition, Whitmore et al. (1993) examined the same sample of 55 rich clusters of Dressler (1980) and showed that the distance from the cluster centre is the driver of galaxy evolution in clusters for all galaxy types.

---

[*] A table of the fitted parameters for each galaxy is only available at the CDS via anonymous ftp to cdsarc.u-strasbg.fr (130.79.128.5) or via http://cdsarc.u-strasbg.fr/viz-bin/cat/J/A+A/633/A104

Despite the extensive studies, the details regarding the key physical mechanisms responsible for the changes in galaxy morphology in dense environments, and how quickly those changes happen with redshift, remain an open issue. Fasano et al. (2000) showed that clusters at $0.1 \leq z \leq 0.25$ are a factor of two to three less abundant in spiral galaxies compared to those at intermediate redshifts while the fraction of S0 galaxies is increasing compared with the results at intermediate redshifts $0.4 \leq z \leq 0.5$ (Dressler et al. 1997; Smail et al. 1997). Moreover, the number of early-type galaxies (ellipticals and S0s) decreases up to $z \sim 1$ (van Dokkum et al. 2000, Lubin et al. 2002). In addition, Postman et al. (2005) and Desai et al. (2007) demonstrated that the decline of early-type galaxies when we move to higher redshifts, namely $z \sim 0.8 - 1$, is the result of the decreasing proportion of S0 galaxies. Finally, Cerulo et al. (2017) found that the red sequence at $z \sim 1$ is dominated by elliptical galaxies at all luminosities and stellar masses while the red sequence of local galaxy clusters becomes dominated by S0 galaxies. This last finding may imply that ellipticals and S0 galaxies follow different evolutionary paths.

A powerful method to characterise galaxy types is to study the structure based on quantification of the integrated light profiles. For instance, one of the most common analytic functions, the Sérsic function (Sersic et al. 1968), quantifies the structure of galaxies in a few parameters such magnitude, the effective radius (R_e), Sérsic index (n), and ellipticity. However, the apparent structure of a galaxy may change as a function of the wavelength since different physical processes dominate the emission at various wavelengths, while the extinction by dust may obscure the central regions of galaxies, greatly affecting the interpretation of the global morphology (MacArthur et al. 2004; La Barbera et al. 2010; Kelvin et al. 2012; Kim & Im 2013; Vulcani et al. 2014; Kennedy et al. 2015; Mosenkov et al., in prep.).

Studying the structure of galaxies in multiple bands and examining how it varies as a function of wavelength enables us to better investigate the physical processes that shape the galaxies. La Barbera et al. (2010) made the first attempt based on a sample of 5080 local early-type galaxies at optical and near-infrared (NIR) wavelengths. These latter authors showed that the Sérsic index does not vary considerably with wavelength while the mean effective radius decreases significantly with increasing wavelength from g to H. Kelvin et al. (2012) divided the Galaxy and Mass Assembly (GAMA, Driver et al. 2009) galaxies into early and late types using optical–near-infrared colours and Sérsic index and showed that there is an observed change in galaxy size as a function of wavelength, which is probably caused by dust attenuation and/or the inside-out growth of galaxies. Vulcani et al. (2014) further investigated the GAMA sample applying a multi-wavelength analysis (the same as the present study) and showed that there is a substantial increase in Sérsic index, and a decrease in effective radius across the same wavelength range. It was proposed that metallicity gradients as well as dust attenuation were the main reasons driving these trends. Kennedy et al. (2015) expanded the Vulcani et al. (2014) study and found that early-type galaxies show little variation in their Sérsic index with wavelength but that they are significantly smaller at longer wavelengths. Late-type galaxies (low-n) display a substantial increase in Sérsic index with wavelength.

In this paper, we build on the previous GAMA studies, which were focused on field galaxies, we use a well-tested methodology of multi-wavelength structural modelling and apply it on optical and NIR imaging of galaxies selected from the WIde-field Nearby Galaxy-cluster Survey (WINGS, Fasano et al. 2006). Furthermore, we combine the derived structural measurements with physical cluster parameters in order to investigate how these affect the observed galaxy morphology. Our goal here is to examine how the galaxy structural properties as a function of wavelength are affected by the local environment.

The paper is organised as follows. In Sect. 2 we present the WINGS survey and the observations we used. In Sect. 3 we present our analysis and we show the final sample. In Sect. 4 we show the dependence of the structural parameters of the galaxies on the wavelength used as well as on their location in the clusters, and compare them with galaxies in the field. In Sect. 5 we compare our results with previous works. Finally, in Sect. 6 we summarise and present our conclusions.

2. The WINGS survey

The WINGS is a wide field multi-wavelength imaging and spectroscopic survey of 77 nearby galaxy clusters (36 in the northern hemisphere and 41 in the south). All clusters are in the redshift range $0.04 < z < 0.07$, have a high Galactic latitude ($|b| < 20$ deg), and have been X-ray selected.

The WINGS survey is the largest survey of nearby galaxy clusters that combines both optical and NIR imaging together with spectroscopic observations. It provides a robust and homogeneous observational dataset suitable for the goals of this study. Previous studies of WINGS provide catalogues with derived measurements such as morphology, local density, distance from the brightest galaxy of the cluster, stellar mass, star formation history, redshift, and cluster membership (see Moretti et al. (2014) for more details on the data). The initial WINGS observations, in B- and V-bands (WINGS-OPT), consist of $\sim$550,000 galaxies. The optical images were taken using the wide field cameras on either the 2.5 m *Isaac Newton* Telescope (WFC@INT) or the MPG/ESO-2.2 m telescope (WFI@ESO). The pixel scales of WFC and WFI instruments are 0.332″ and 0.238″, respectively, and they cover a field of view (FoV) of $34' \times 34'$. Additional B- and V-bands images were obtained from the wide-field imager OmegaCAM ($\sim$1 degree) of the VLT Survey Telescope (VST) on Paranal.

Near-infrared observations of the WINGS survey (WINGS-NIR) were performed with WFCAM@UKIRT and they contain $\sim$500,000 galaxies. The NIR imagery has a pixel scale of 0.2″ and a corresponding FoV of 0.79 degrees. A broad U-band imaging of a subsample of the WINGS clusters has also been obtained with wide-field cameras at different telescopes (INT, LBT, Bok, see Omizzolo et al. 2014). The pixel scale of U-band images is 0.21″.

Furthermore, spectroscopic information is available for 48 of the WINGS clusters with a high degree of completeness. The spectroscopic observations were obtained with the AF2/WYFFOS multifibre spectrograph mounted on the 4.2 m *William Herschel* Telescope (WHT) and the 2dF multifibre spectrograph of the 3.9 m Anglo Australian Telescope (AAT; Cava et al. 2009). Cava et al. (2009) calculated the redshift of individual galaxies based on a semi-analytical method that identifies the emission lines of the spectrum.

Vulcani et al. (2012) computed the projected local densities for the clusters, Σ_N, which is commonly defined as the number of neighbours (N_n) of each galaxy per Mpc^2. These latter authors identified the ten nearest neighbours of each cluster galaxy with $M_V \leq -19.5$ and calculated $\Sigma_{10} = 10/A_{10}$, using a circle to define the area including these neighbours, where $A_{10} = \pi(R_{10})^2$ (Mpc) and R_{10} (Mpc) is the radius in Mpc of the smallest circle centred on the galaxy. Fritz et al. (2007, 2011) calculated the integrated stellar masses for a subsample of 5229 WINGS

Table 1. Cluster properties and number of member and non-member galaxies of each galaxy cluster.

Cluster	α J2000	δ J2000	z	No. of cluster galaxies	No. of non-member galaxies	No. of cluster galaxies ($M_V < -19.27$ mag)
(1)	(2)	(3)	(4)	(5)	(6)	(7)
A0119	00 56 21	−01 15	0.0442	144	33	72
A0500	04 38 52	−22 06	0.0670	80	33	39
A1291	11 32 21	55 58	0.0527	12	20	4
A1631a	12 52 52	−15 24	0.0466	132	28	43
A1983	14 52 59	16 42	0.0444	19	15	8
MKW3s	15 21 52	07 42	0.0453	25	10	13
A2382	21 51 55	−15 42	0.0644	162	55	69
A2399	21 57 13	−07 50	0.0582	112	45	40
A2457	22 35 41	01 29	0.0591	104	15	50

Notes. Columns: (1) Galaxy cluster name. (2) Right ascension. (3) Declination. (4) Redshift. (5) Number of member galaxies in each galaxy cluster (no absolute magnitude cut). (6) Number of non-member galaxies (with $z < 0.15$ and $M_V < -19.27$ mag) in each galaxy cluster. (7) Number of member galaxies in each galaxy cluster (with $M_V < -19.27$ mag).

galaxies via spectro-photometric modelling. They used the fibre spectra and the fibre and total magnitudes to derive the stellar masses, luminosity-weighted and mass-weighted ages, average star formation rates, as well as the fibre and total magnitudes pertaining to the best fit model. The morphological classification is based on MORPHOT (Fasano et al. 2012), a tool for automatic galaxy morphology that used to classify ~30.000 galaxies of the WINGS survey (Fasano et al. 2006). MORPHOT produces two different morphological estimates based on a semi-analytical maximum likelihood technique and a neural network machine. For more details about the WINGS survey see also Varela et al. (2009), Valentinuzzi et al. (2009), Poggianti et al. (2009), Vulcani et al. (2011a,b, 2013), D'Onofrio et al. (2014).

For the purpose of this study we use nine WINGS clusters with available imaging in at least four bands as well as spectroscopic redshift measurements. Table 1 lists the available images for each cluster, the cluster name, coordinates, redshift, the available images, and the number of member and non-member galaxies of each galaxy cluster that have been successfully fitted by our analysis.

3. Analysis

Given the size and the complexity of the datasets used we present in detail the necessary steps taken for the analysis.

3.1. Rescaling the images

The multi-wavelength fitting process performed in this study requires all images to be in the same resolution and to cover the same area of the sky. To perform this, we use the MONTAGE software (Berriman et al. 2008). First, all images are converted to the same pixel scale using as a reference the pixel scale of the K-band and then they are cropped to the size of the smallest image, namely the V-band image. We then correct for flux conservation by multiplying each optical image for the factor $(pix.scale_{K-band}/pix.scale_{opt.band})^2$. We convert all the optical images to counts multiplying each optical image with the given exposure time, as required by GALFITM. Finally, we crop the images of each cluster in tiles of 2000×2000 pixels with an overlap of 500 pixels (49 tiles at each band; described in the following section) to speed up the subsequent processing by GALAPAGOS (Barden et al. 2012) We note that we calculate the zero point of each band based on the counts format.

3.2. Creating different point spread functions

Since the point spread function (PSF) varies depending on the physical location on the focal plane, we construct different PSFs along the x- and y-axes of the images for each band. We rely on the PSF Extractor code for this task (see Bertin et al. 2011, PSFEx) as well as the description of SExtractor (Bertin & Arnouts 1996). SExtractor detects sources, and provides both photometric and shape information for all of them, which can be used by PSFEx to identify a clean sample of sufficiently bright stars. We then PSFEx to each image and construct 14x14 PSFs per filter and field based on a regular grid, as is usually done by PSFEx. This means that the typical distance between PSFs is 700 pixels. Using the analysis plots provided by PSFEx, we made sure that none of the PSF parameters such as FWHM or ellipticity change significantly on such a scale. Point spread functions were also visually inspected for any abnormal features. GALAPAGOS offers the possibility to use such a grid by choosing the closest PSF to each object for its fit. This way, it is assured that the optimum PSF is used at all times.

3.3. Using the GALAPAGOS software

GALAPAGOS (Barden et al. 2012) is an Interactive Data Language (IDL) wrapper of GALFIT (Peng et al. 2002) and SExtractor (Bertin & Arnouts 1996) that enables the automated detection and structural analysis of galaxies in a typically large image. GALAPAGOS uses SExtractor to detect sources in the data, estimates a local sky background, cuts postage stamp images for all sources (smaller sections of the inputs images centred on individual sources, with dimensions based on the Kron radius of the source), prepares object masks, performs Sérsic fitting taking into account light contamination from neighbouring sources, and compiles all objects in a final output catalogue. In our study we make use of the updated version GALAPAGOS-2 (Häußler et al. 2013) which uses a multi-wavelength version of GALFIT, named GALFITM, developed by the MegaMorph team (Bamford et al. 2012; Häußler et al. 2013; Vika et al. 2013, 2014, 2015).

We chose the V-band for detecting the sources for each cluster as it is deeper than the others. The High Dynamic Range (HDR) mode of GALAPAGOS (Barden et al. 2012) detects the sources in two stages. First, the "cold run" detects (but does not split up) all bright objects; the second, "hot" run detects

fainter sources. In addition, we changed the keywords in the first block of GALAPAGOS-2 (cold and hot configuration files of HDR SExtractor source detection) in order to improve the splitting effect of cluster galaxies according to the image specifications of the WINGS survey. After combining the cold and hot catalogues, GALAPAGOS-2 provides the data for an easy visual inspection. In this step it is easy to flag any misdetections (split up objects or fake detecting), which can be removed from any future part of the code. In this work, we examined all detections to ensure that all such misdetections are correctly flagged up. For each detection, GALAPAGOS-2 cuts the science images into postage stamps. It also provides the sky background very efficiently using a flux growth method to estimate the local sky around an object (see Barden et al. 2012). GALAPAGOS-2 applies GALFITM in each postage stamp and models the light distribution of the central source. It is worth noting that GALAPAGOS-2 masks out distant and faint neighbours. Reasonably bright neighbouring sources that can affect the model of the central source are fit simultaneously.

In addition, we make use of the GALAPAGOS-2 feature that masks the deblending sources. Finally, we visually inspect the whole FoV of each band after the detection process to confirm that there is no artificial splitting of a single source.

After the fitting process, GALAPAGOS-2 creates a catalogue with all calculated parameters from SExtractor and GALFITM. For more details on the software performance, see Häußler et al. (2013).

The fitting process is performed with GALFITM, which uses the Levenberg-Marquardt (LM) algorithm to minimise the residual between a galaxy image and the PSF-convolved model by modifying the free parameters. In our setup we use the sigma images internally created by GALFITM. For this study we use images of five different wavelengths in optical and NIR. As a first step, GALFITM fits a single wavelength-dependent model to all images. A second step allows for bulge/disk decomposition, but as this feature is not being used in this work, we do not discuss it here. The model comprises a single-Sérsic function, with a number of parameters: for example, centre position (xc, yc), magnitude (m), effective radius (R_e), Sérsic index (n), axial ratio (Q), and position angle (PA).

The magnitude input (m_{input}) or starting value to GALFIT is the SExtractor MAG BEST for the V-band image and typical offsets for the other images. These offsets for each band are calculated to adjust the average magnitudes measured on the V-band detection image to those for individual bands. We allow full freedom in magnitudes, while we allow the Sérsic index and R_e to vary with wavelength linearly (as first-order polynomials). We also explored a quadratic variation of the Sérsic index and R_e with wavelength but did not observe significant changes in the structural parameters. Since we have only five bands for the majority of clusters, we decided to allow the smallest variation of the structural parameters with wavelength. Moreover, allowing a minimal degree of freedom we optimally use the advantages that GALFITM offers.

The galaxy centre position, the position angle, and the axis ratio are chosen to be constant with wavelength.

There are multiple advantages of simultaneously using multiple images for modelling the light distribution of a galaxy, such as increasing the overall signal-to-noise ratio and using the colour difference between the components to support decomposition. By constraining the variation freedom for some parameters, the statistical uncertainty of the effective radius, Sérsic index, and magnitude is reduced (Häußler et al. 2013).

3.4. Sample selection

We validate the GALAPAGOS-2 catalogue in order to select only the objects that have been successfully modelled. In particular, each source with one or more parameters lying on (or very close to) a fitting constraint has been discarded.

The only galaxies kept in our analysis are those that satisfy the following criteria, as recommended by Häußler et al. (2013) and Vika et al. (2013).

- $0 < m < 40$ at all wavelengths, where m is the total apparent output magnitude in each band.
- $m_{input} - 5 < m < m_{input} + 5$, where m_{input} is the starting value of the magnitude in each band. These are derived by scaling an average galaxy spectral energy distribution (SED) by the MAG BEST value measured by SExtractor during object detection. During the fit, we allow a generous variation of ± 5 magnitudes from these starting values.
- $0.201 < n < 7.90$, since fits with values outside these ranges are rarely meaningful and very close to the constraints used during the fit.
- $0.301 < R_e < 399.0$ pixels, which maintains values in a physically meaningful range and prevents the code from fitting very small sizes, where the fitting iterations become very slow due to oversampling issues.
- $0.1 < Q \leq 1.0$, where Q is the axis ratio in order to ensure the fit value is physically meaningful.

Finally, we clarify to the reader that the total number of galaxies excluded due to GALAPAGOS-2 constraints are 13 member galaxies and 9 non-member galaxies (2% of our sample, thus not affecting the uncertainty on the fitted parameters). Equally, we can argue that all our constraints are conservatively chosen to be so wide that they only help to avoid unphysical areas of parameter space.

We focus on galaxies with secure structural parameters, redshift measurements (Cava et al. 2009), and morphological classifications (Fasano et al. 2012). Figure 1 presents the B–V colour and total stellar mass distributions for the galaxies inside the nine clusters of our sample.

In addition, in order to be consistent with geometrical biases, we limit our analysis to the minimum radius imaged for all clusters ($0.64 \times R_{200}$).

Our galaxy sample consists of 1044 galaxies, 790 of which are spectroscopically confirmed members. The remaining galaxies (254) constitute our non-members sample. These latter might simply be field galaxies close to the clusters, or they could indeed be galaxies in small groups that will soon fall into the clusters. The separation of cluster and non-member galaxies was published in Cava et al. (2009) and Moretti et al. (2017); we use the published results. The absolute V magnitude (M_V) and the redshift range of cluster and non-member galaxies of our sample are presented in Fig. 2. Table 2 provides the number of cluster and non-member galaxies in each cluster for each morphological class.

In order to study the difference between cluster galaxies and non-member galaxies we created a secondary sample by applying the following selection criteria: redshift $z \leq 0.15$, which corresponds to $M_V < -19.27$ mag. This redshift cut helps to avoid galaxy evolution effects (Fig. 2) but at the same time allows for a sufficient number of galaxies to be included in the non-member sample. These criteria select 338 cluster galaxies and 254 non-member galaxies. This second sample is only used in Sect. 4.4.

Based on the Fasano et al. (2006) classification (also Calvi et al. 2013 used this), we define as elliptical galaxies (E) those that have Hubble type (T) between -5.00 and -4.25, lenticular
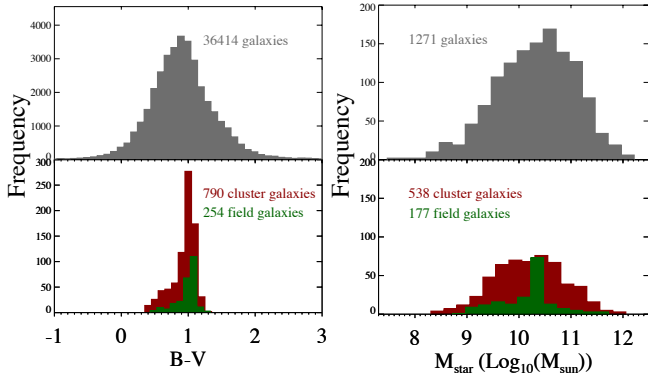
Fig. 1. *Left panel*: B–V colour and total stellar mass distributions for the galaxies inside the nine clusters. On the upper panel we show the distribution for all WINGS galaxies of the nine clusters (grey colour) with available B–V colours from Varela et al. (2009) and at the *bottom* we show the histogram of the galaxies of this study (red for cluster galaxies and green for non-member galaxies). *Right panel*: same as on the left, but for the stellar mass. Galaxies of this study have secure structural parameters (available redshift measurements and available morphological classifications). The fact that the total number galaxies of this study (790) is much smaller than the 36414 galaxies of Varela et al. (2009) is due to the lack of spectroscopic data and morphological classification values. The lack of spectroscopic measurements is also responsible for the small number of galaxies (1271) with available stellar mass estimates. Our sample includes the majority (more than 95%) of galaxies (both cluster members and non-members) that have spectroscopic measurements.
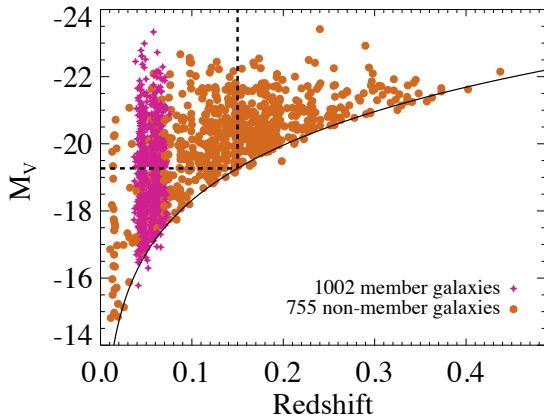
Fig. 2. Absolute *V*-band magnitude vs. redshift for the detected galaxies (cluster and non-members). Pink stars indicate the member galaxies while the brown circles are the non-member galaxies. The curved line indicates the spectroscopic apparent magnitude limit of WINGS, $V \sim 20.0$. The dashed vertical line represents the redshift cut at 0.15 while the horizontal dashed line indicates the $M_V = -19.27$.

galaxies (S0) those with $T \geq -4.25$ and $T \leq 0$, early-type spirals those with $T > 0$ and $T \leq 4.00$, and late-type spirals the remaining galaxies ($T > 4.00$).

We remind the reader that our sample is a magnitude-limited sample ($m_V \sim 20$ mag). We use all cluster galaxies (independent of their luminosity) to study their properties inside local clusters. In order to check if we are consistent with the completeness in luminosity and stellar mass we we measure the ratio between the maximum and the minimum distance of the clusters (301 Mpc/195 Mpc) ~ 1.54.). The difference in flux for those extreme clusters is equal to 2.38 which is interpreted as a difference of 0.94 in magnitude. The ratio in the luminosity limit

Table 2. Number of cluster and non-member galaxies in each cluster for each morphological class.

Cluster	Ellipticals	S0s	Early-type spirals	Late-type spirals
A0119	50 (28) [8]	82 (37) [11]	12 (7) [13]	– (–) [1]
A0500	23 (15) [9]	38 (15) [8]	14 (5) [12]	5 (4) [4]
A1291	2 (–) [4]	7 (1) [9]	3 (3) [7]	– (–) [–]
A1631a	22 (9) [2]	60 (23) [10]	39 (11) [11]	11 (–) [5]
A1983	4 (1) [5]	9 (5) [6]	6 (2) [4]	– (–) [–]
MKW3s	7 (5) [2]	13 (6) [3]	4 (2) [4]	1 (–) [1]
A2382	34 (16) [8]	55 (29) [20]	51 (18) [17]	22 (6) [10]
A2399	18 (8) [6]	42 (15) [13]	39 (16) [14]	13 (1) [12]
A2457	29 (15) [3]	54 (23) [5]	18 (12) [6]	3 (–) [1]

Notes. The sample of cluster-member galaxies, cluster-member galaxies with $M_V < -19.27$ mag (inside parenthesis), and non-member galaxies (inside square brackets) of the nine galaxy clusters. Columns: (1) Galaxy cluster name. (2) Number of elliptical galaxies. (3) Number of lenticular (S0) galaxies. (4) Number of early-type spiral galaxies. (5) Number of late-type spiral galaxies.

will be equivalent to this latter. As for the stellar mass, we use the formula of Bell et al. (2003) ; $M(M_\odot) \sim 0.95 \pm 0.03 \times L_{K_\odot}$ and we find that the change in mass function sampling will also be a factor of $\sim$2.38 (depending on the B–R colour corrections). However, the variation of structural parameters as a function of wavelength does not change if we use bright cluster galaxies (with $M_V < -19.27$ mag). For instance, the average n values become larger while the average R_e decreases.

At this point, we should mention that since no *J*-band images are available four out of nine galaxy clusters we had to ensure that this did not introduce bias to our results. For this reason, we ran our code on the galaxies in the clusters that have five available bands after removing the *J*-band, and we found no difference in the observed trends of n and R_e.

Finally, for those galaxies that lack *u*- or *J*-band measurements, we estimated the *u*- and *J*-band Sérsic index and effective radius from the results of *B*-, *V*-, and *K*-band taking into consideration that the structural parameters vary linearly as a function of wavelength.

Our results can be found in electronic form at the CDS.

4. Results

Since the stellar mass distribution is not the same for different morphological galaxy types (Vulcani et al. 2012), we examined the dependence of the structural parameters (Sérsic index and R_e) of the cluster galaxies on the stellar mass. It is obvious that in Fig. 3 there is a clear trend, especially for ellipticals and lenticulars, between Sérsic index and stellar mass. More massive early-type galaxies (ellipticals and S0s) have larger Sérsic index values, while spiral galaxies have Sérsic index values in the range 0.5–1.5, independent of their total stellar mass. On the other hand, Fig. 4 presents the dependence of R_e on the stellar mass for all morphological types, and as expected more massive galaxies display higher R_e values. The stellar masses in Figs. 3 and 4 are derived from Fritz et al. (2011). Since, spectroscopic measurements are not available for all WINGS clusters, some galaxies lack published stellar masses. The stellar masses, star formation histories, extinction values, and average stellar ages of galaxies were derived by analysing the integrated spectra of galaxies by means of spectral synthesis techniques.
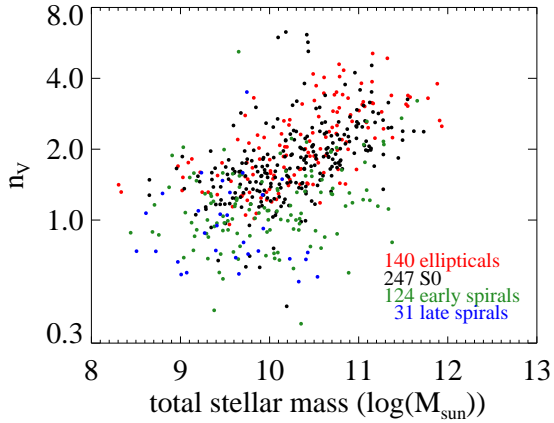
Fig. 3. Sérsic index in *V*-band as a function of the total stellar mass of the cluster galaxies sample up to $0.64 \times R_{BCG}$. The total number of the cluster members in this figure is lower because not all of them have available stellar mass measurements.
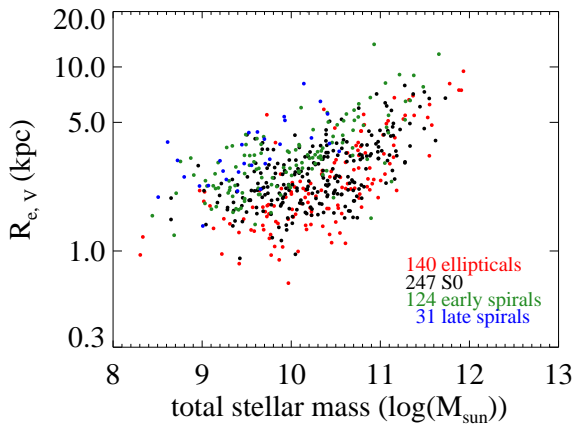

Fig. 4. R_e in *V*-band as a function of the total stellar mass of the cluster galaxies sample up to $0.64 \times R_{BCG}$. The colour coding and description is the same as in Fig. 3.

4.1. The Sérsic index of cluster members in the optical and NIR

In Fig. 5 we present a histogram of the Sérsic index for the confirmed cluster member galaxies in the five bands. Elliptical galaxies have on average the largest Sérsic indices in all bands. Lenticulars (the most abundant galaxy type in our sample) display Sérsic indices similar to ellipticals but smaller on average. Early and late-type spirals have Sérsic indices closer to 1 with the late-type spirals having smaller values on average. We note that the scatter for the ellipticals and lenticulars is partially due to the nature of the sample that includes galaxies with different stellar masses as seen in Fig. 3.

In the top panel of Fig. 6 we present the weighted median *n* of the cluster galaxies as a function of wavelength for the same four morphological types. Error bars show the uncertainty of the median (calculated as $1.253\sigma/\sqrt{N}$), where σ is the standard deviation and N is the number of galaxies in the sample. The spectroscopic weight for each sample galaxy analysed is the inverse of the magnitude completeness factor $C(m)$ (see details in the Appendix B of Fritz et al. 2014). The weighted median value of our study is computed as follows: We sort the structural parameters of a sample and their spectroscopic weights. We normalise the spectroscopic weights dividing by the total of the weights, such that:
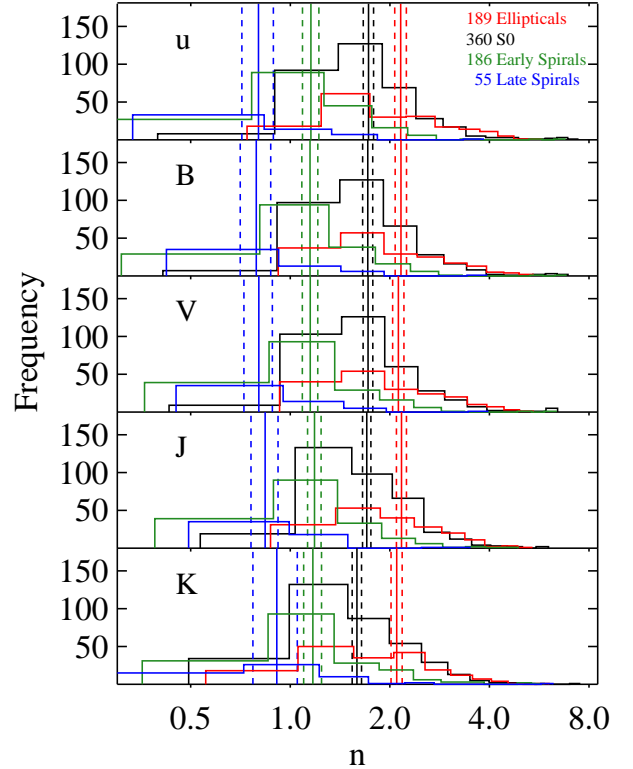
Fig. 5. Distribution of the Sérsic index for the different bands for the cluster galaxies sample. Ellipticals, S0s, and early- and late-type spirals are in red, black, green, and blue lines, respectively. The vertical solid and dashed lines show the weighted median values and their corresponding uncertainty of each galaxy type calculated as $1.253\sigma/\sqrt{N}$, where σ is the standard deviation and N is the number of galaxies in the sample. The legend indicates the number of galaxies per type.

$$\sum_{i=1}^{n} w_{i,\text{spec}} = 1. \tag{1}$$

The weighted median of the sample is the k-element parameter that satisfies the two conditions:

$$\sum_{i=1}^{k-1} w_{i,\text{spec}} \leq 1/2, \tag{2}$$

and

$$\sum_{i=k+1}^{n} w_{i,\text{spec}} \leq 1/2. \tag{3}$$

In the top panel of Fig. 6 we see that the weighted median *n* of ellipticals and early-type spirals remains constant from the *u*-band to the *K*-band. Here we can see that S0s have similar *n* values from *u*- to *J*-band with slightly lower values in the *K*-band, while late-type spirals tend to display larger values in the *K*-band compared to the remaining bands. We applied a Kolmogorov-Smirnov (K–S) test on the unbinned data of late-type spirals in the top panel of Fig. 6. The corresponding probability of the K–S distribution between *K*- and the other bands (*u*, *B*, *V* and *J*) is (0.57, 0.42, 0.42, 0.88). From the previous KS test probabilities we cannot conclude if the Sersic index estimated in the *K*-band is different (or comes from the same sample) from the other bands. We therefore conclude that the median values of the Sérsic index of late-type spirals remain constant from optical to NIR wavelengths.

In the middle panel of Fig. 6, we examine how the Sérsic index changes as a function of the wavelength, but this time
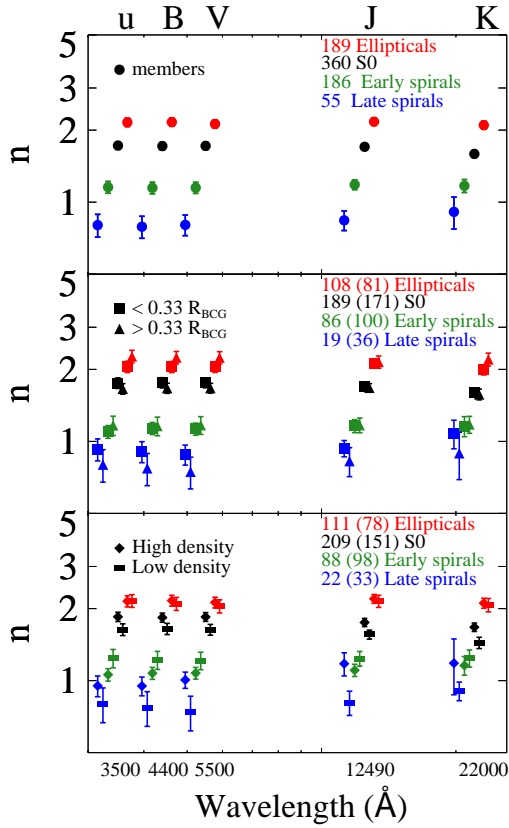
Fig. 6. Weighted median n as a function of wavelength for different morphological types of galaxies. Colour coding is the same as in Fig. 5. The error bars show the uncertainty of the median (calculated as $1.253\sigma/\sqrt{N}$, where σ is the standard deviation and N is the number of galaxies in the sample). The x-points are slightly shifted along the wavelength axis in order to make the errors readable. The numbers before the parenthesis show the total number of each galaxy type that are located in the inner region (*middle panel*) and inside high-local-density regions (*bottom panel*). The numbers inside parentheses denote the total number of each galaxy type that are in the outer region (*middle panel*) and inside low-local-density regions (*bottom panel*).

after splitting the sample of the cluster member galaxies based on their distance from the centre of the corresponding cluster. Following the definition of Cava et al. (2009), the R_{BCG} of a galaxy is the projected distance from the brightest cluster galaxy (BCG). The R_{BCG} is normalized into R_{200}[1] units. Following the findings of Fasano et al. (2015), we divide the area of the clusters into two regions: the inner region, which extends out to $0.33 \times R_{200}$, and the outer region, which is beyond this limit. We find that the inner region contains 402 cluster member galaxies (108 ellipticals, 189 S0s, 86 early-type spirals, and 19 late-type spirals) while the outer region consists of 388 galaxies (81 ellipticals, 171 S0s, 100 early-type spirals, and 36 late-type spirals).

It appears that the average n of elliptical and early-type spirals remains the same independent of the location of the galaxies at the inner or outer regions of clusters and does not change as a function of wavelength. However, lenticulars and late-type spirals located in the outer region of clusters have a slightly smaller average n in all five bands compared to the galaxies in

the inner region of the clusters. Additionally, lenticulars located in the outer region of clusters show a drop of their average n as we move from optical to NIR bands, while late-type spirals located in the inner part of the clusters show an increase of their average n.

In the lower panel of Fig. 6 we split the sample based on the density of the environment where a cluster galaxy is located. The first group found in regions with high projected local densities ($\log(\Sigma_{10}) > 1.45$) contains 430 cluster galaxies (111 ellipticals, 209 S0s, 88 early-type spirals, and 22 late-type spirals) while the second, found in regions with low projected local densities ($\log(\Sigma_{10}) < 1.45$), contains 360 cluster galaxies (78 ellipticals, 151 S0s, 98 early-type spirals, and 33 late-type spirals). The values of the projected local density for each galaxy as well as the local density limit are based on the findings of Fasano et al. (2015). We see that the projected local density is a cluster physical parameter that differentiates the average n for all morphological types with the exception of the ellipticals. Here we can see that S0s and late-type spirals have average n larger in denser environments, while early-type spirals show the opposite trend. We applied K–S tests for all morphological types of galaxies to examine the results in the following manner: We compared all the elliptical galaxies (unbinned data) that were found in high-density regions against the ellipticals that reside in the low-density regions. We repeated the same approach for the lenticulars, and early- and late-type spirals.

In particular, ellipticals do not change their average n values as a function of wavelength (K–S test probability = 0.05) in either high- or low-projected-density regions. The Sérsic of lenticulars displays a decrease in J- and K-band that is stronger for galaxies found in low-density environments. The Sérsic index of early-type spirals changes as a function of wavelength for regions with different projected local densities (K–S test probability = 0.005) in both high- and low-projected-density regions. Late-type spirals found in both low- and high-density environments show a trend as a function of wavelength, where the average Sérsic index increases as we move from u- to K-band but with an increase in the scatter as well. The probabilities of a K–S test on S0s and late-type spirals concerning low and high local densities are extremely low ($<10^{-5}$).

4.2. The effective radius of cluster member galaxies in the optical and NIR

Figure 7 presents the distribution of the effective radius (R_{e}) for the different bands for our cluster-member sample. The R_{e} of each galaxy has been converted to physical units (kpc) using the radial velocity (Cava et al. 2009) for each galaxy. Spirals have the larger values of R_{e} in all bands while the ellipticals and S0s have the smaller R_{e} in all bands. The general trend for all types of galaxies is that the weighted median R_{e} decreases from the optical to NIR wavelengths.

In the top panel of Fig. 8 we show the weighted median R_{e} of the cluster-member galaxies. All morphological types show a decrease of their average R_{e} as a function of the wavelength with the elliptical and the early-type spiral to show the larger change.

In the middle panel of Fig. 8 we show how the effective radius changes as a function of wavelength for the galaxies located in the inner and outer regions of the clusters. The sample separation is the same as in Sect. 4.1. We notice that elliptical, lenticular, and early-type spiral galaxies have the same average R_{e} independent of their location in the cluster. However, late-type spiral galaxies appear to have smaller average R_{e} when they

---

[1] R_{200} is defined as the radius delimiting a sphere with interior mean density 200 times the critical density, approximately equal to the cluster virial radius.
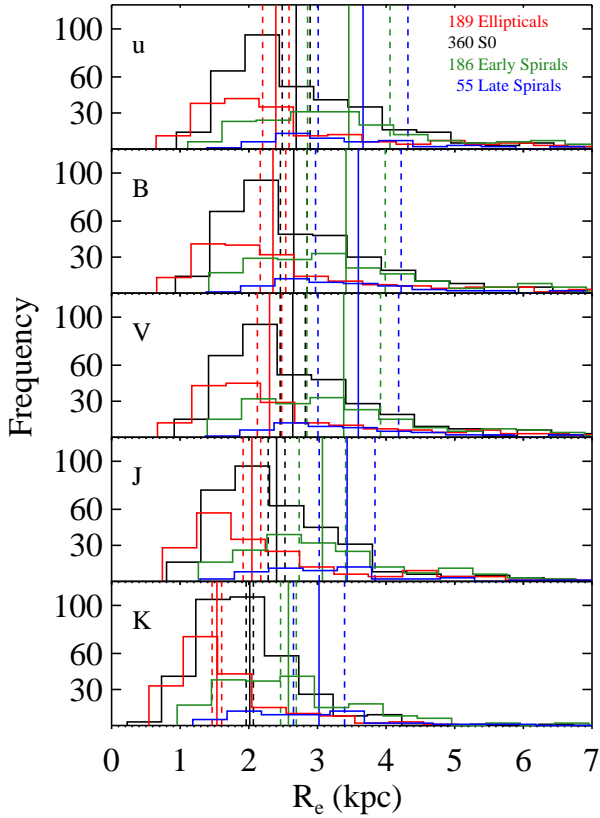
Fig. 7. Distribution of R_e for the different bands for the cluster member galaxies. The colour coding and description are the same as in Fig. 5.
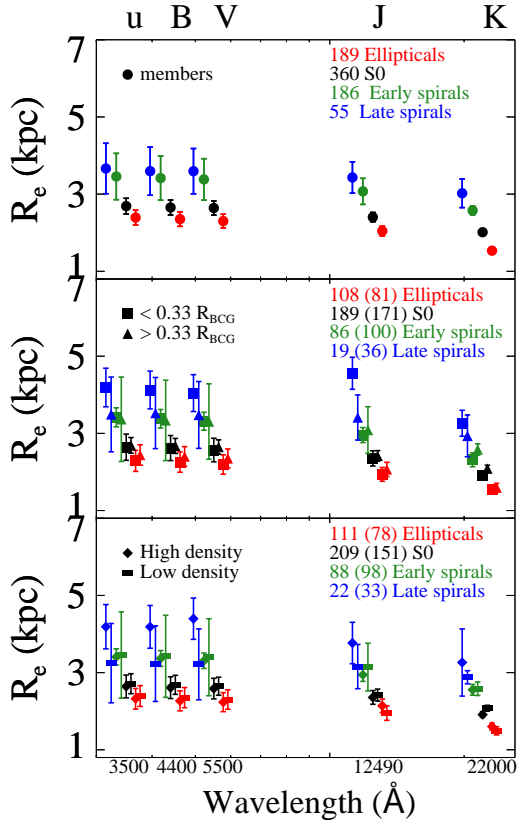
Fig. 8. Weigthed median R_e as a function of wavelength for different morphological types of galaxies. The colour coding and description are the same as in Fig. 6.

are in the outer area of the cluster, even though the difference is within the error bars.

In the bottom panel of Fig. 8 we examine how the R_e of the cluster members changes in regions with low and high projected local densities. We see that for all galaxy types (except for the late-type spirals) there is no difference in the weighted median R_e values in regions with high and low projected local densities. The median value of late-type spirals R_e is larger in higher local densities rather than in regions with lower local densities. A KS test analysis reveals that the probability that low- and high-density late-type galaxies are drawn from the same sample is 0.004 (p-statistic equal to 1.00), which supports this latter result. However, this is not the case for the other galaxy types, since the KS p-statistics are equal to 0.70, 0.21, and 0.69 (D values are equal to 0.40, 0.60, 0.40) for ellipticals, S0s, and early type spirals, respectively.

4.3. Dependence on the distance from the BCG and the projected local density

In this section we examine how n and R_e change as a function of the projected distance from the cluster centre (R_{BCG}) and the projected local density (Σ_{10}). In Fig. 9 we show the median values of n in u-, V-, and K-band as a function of R_{BCG}. We do not show the results of the B- and J-band as they are practically identical to those of V- and K-band, respectively. Elliptical, lenticular, and early-type spiral galaxies have statistically constant n values in all bands with late-type galaxies showing the smallest scatter. In late-type spiral galaxies the average n decreases up to $0.3 \times R_{200}$ and remains constant within the errors further out. To investigate the robustness of the trend, we applied a linear least-square fit to explore the dependence of R_{BCG} as a function of the Sérsic index for the unbinned data of late-type spirals that are located in $[0.0–0.35] \times R_{200}$, and examined the uncertainty due to the scatter of the points, the intercept, and the slope coefficients. We find that for the u-band, the intercept and slope are: 1.5 ± 0.18, and -2.54 ± 0.66, while for the V-band they are 1.45 ± 0.15 and -2.26 ± 0.57. We performed a second linear least-square fit to the unbinned data of late-type spirals located in $[0.09–0.35] \times R_{200}$ excluding the only late-type galaxy found within $[0.0–0.1]$ in order to examine the trend with higher accuracy. We found that for the u-band the corresponding intercept and slope are 1.39 ± 0.23 and -2.16 ± 0.83, while for the V-band they are: 1.38 ± 0.20 and -2.00 ± 0.72. This suggests that the trend is consistent within 3σ (u: $2.6 < 3$; and V: $2.78 < 3$) for galaxies located in $[0.0–0.35] \times R_{200}$. At the largest distances from the cluster centre the Sérsic index for late-type galaxies remains nearly constant.

In Fig. 10 we examine the R_e as a function of the distance from the BCG in optical and NIR. Elliptical and lenticular galaxies have relatively constant R_e values in all bands. In early- and late-type spiral galaxies the R_e shows an increasing trend from the centre out to $[0.3–0.4] \times R_{200}$ in all bands, decreasing further out, even though the errors are large. In order to investigate that trend, we examined again the coefficients of a linear least-square fit for the unbinned data of early- and late- type spirals that are located in $[0.0–0.35] \times R_{200}$ and in $[0.35–0.64] \times R_{200}$. We found that the early-type spirals show no correlation across R_{BCG}, with the following values for the intercept and slope: u-band: 3.30 ± 0.56 and 1.40 ± 2.34, V-band: 3.17 ± 0.53 and 1.45 ± 2.20, K-band: A = 2.17 ± 0.41 and 1.81 ± 1.69. In contrast, late-type spirals show hints of an increase for R_e up to $0.35 \times R_{200}$, since the intercept and slope are in the u- band: 2.30 ± 1.07 and 6.73 ± 3.98, while in the V-band: 2.18 ± 1.02 and
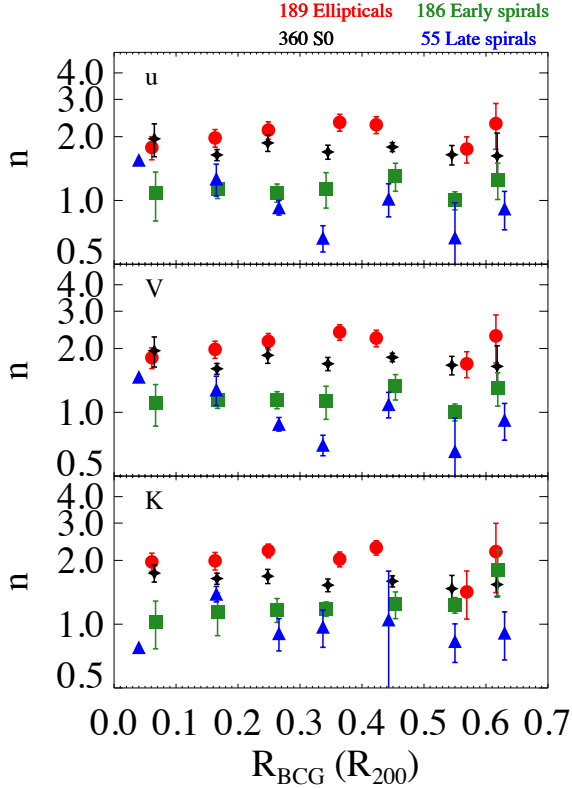
Fig. 9. Weighted median values of n in u-, V-, and K-band as a function of R_{BCG}. The values of R_{BCG} are normalized into R_{200} units and the x-axis is divided into R_{BCG} bins of $0.1 \times R_{200}$. The error bars of each galaxy type in each bin are calculated as $1.253\sigma/\sqrt{N}$, where σ is the standard deviation and N is the number of galaxies of each galaxy type in each bin. The x-points are slightly shifted in order to make the errors more readable and the colour coding is the same as in Fig. 5. Points with no error bars are those with one galaxy inside the corresponding bin. We note that the number of galaxies per bin is not constant (see Table 3).

Table 3. Statistical values per bin for each morphological class of galaxies shown inside the Figs. 9 and 10.

Morphological class	Minimum	Maximum	Mean
Ellipticals	7	37	27
S0s	12	81	51
Early-type spirals	6	40	27
Late-type spirals	1	13	8

Notes. Minimum, maximum, and mean values of each morphological class of galaxy inside bins of Figs. 9 and 10.

6.74 ± 3.78. Especially in K-band, the increase of R_e is more significant with an intercept of 1.15 ± 0.66 and slope 6.82 ± 2.49.

Figure 11 presents the median values of n in the u-, V-, and K-band as a function of the projected local density. Ellipticals, S0s, and early-type spirals have no significant variation in their n values, contrary to the late-type spirals where n appears to increase in particular in the optical bands. For the latter, we applied a spearman rank test on the unbinned data of late-type spirals. In optical bands (u,V) we do not see a clear trend. The rank correlation coefficient for u- and V-band is close to zero. Regarding the K-band, (where we trace well the stellar mass of the galaxies, so the bulge is more prominent) we see that there is a weak trend (rank correlation coefficient is 0.3 and the two-
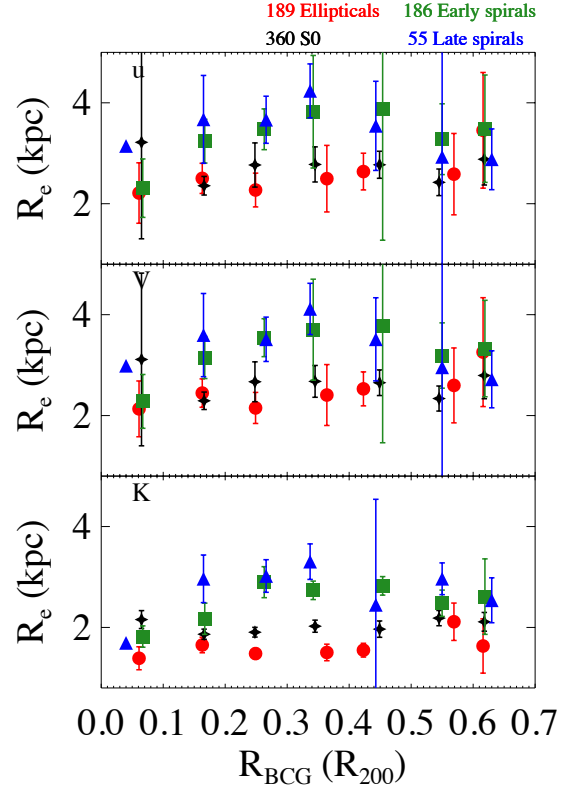
Fig. 10. Weighted median values of R_e in the u-, V-, and K-band as a function of R_{BCG}. The colour coding and description are the same as in Fig. 9 We note that the number of galaxies per bin is not constant (see Table 3).

sided significance of its deviation from zero (p statistic) is 0.025) suggesting a slight increase of the Sérsic index with projected local density.

In Fig. 12 we show the median values of R_e in the u-, V-, and K- band as a function of the projected local density. It is clear that the scatter of R_e in all galaxy types is large. Even though, ellipticals and S0s do not change their size as a function of the local density in all wavelengths, while late-type spiral galaxies tend to have larger R_e in regions with very large local-density values. We applied a spearman rank test on the unbinned data of early- and late-type spirals. The rank correlation coefficient has low values in all bands and the significance of the relation between R_e and local density is very low both for early- and late-type spirals. Furthermore, we investigated the effect of stellar mass on the n and R_e versus projected local density. We divided the sample using a stellar mass cut of $\log_{10}(M_\star) = 10$. We applied spearman tests on the spiral galaxies in u-, V-, and K-band. We observed a weak trend in the K-band for late-type spirals with high values of stellar mass. For that reason, we applied a Spearman test and we found that the Spearman coefficient is equal to 0.6 and the p-statistic is not very small (0.21). We conclude that the R_e of high-stellar-mass late-type spirals and local density in the K-band do not show a correlation.

4.4. Structural properties of cluster members and non-member galaxies

4.4.1. The Sérsic index, n

As we discussed earlier (see Sect. 3.4) in addition to the cluster member galaxies, our imagery also includes some galaxies that are located close to the clusters. We can use these non-member
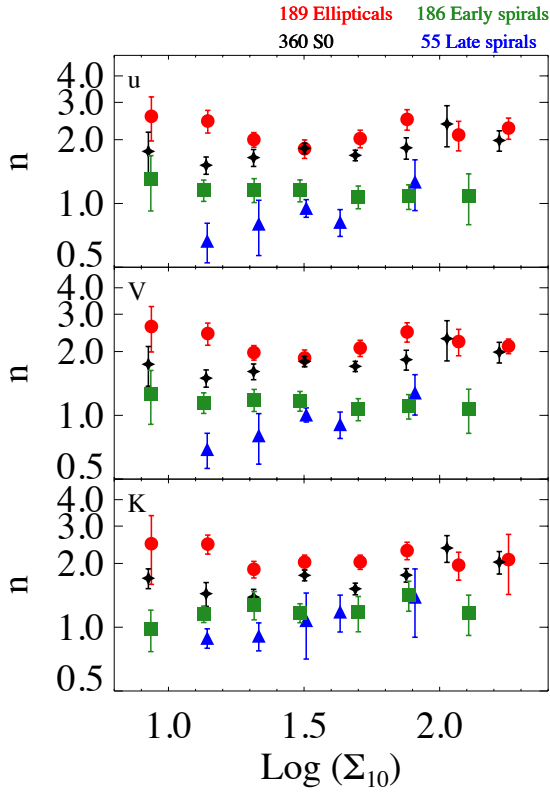
Fig. 11. Weighted median values of *n* in the *u*-, *V*-, and *K*-band as a function of the projected local density of the clusters. We divide the *x*-axis into projected local density bins of $0.2 \times \log(\Sigma_{10})$. The colour coding and description are the same as in Fig. 9. We note that the number of galaxies per bin is not constant (see Table 4).
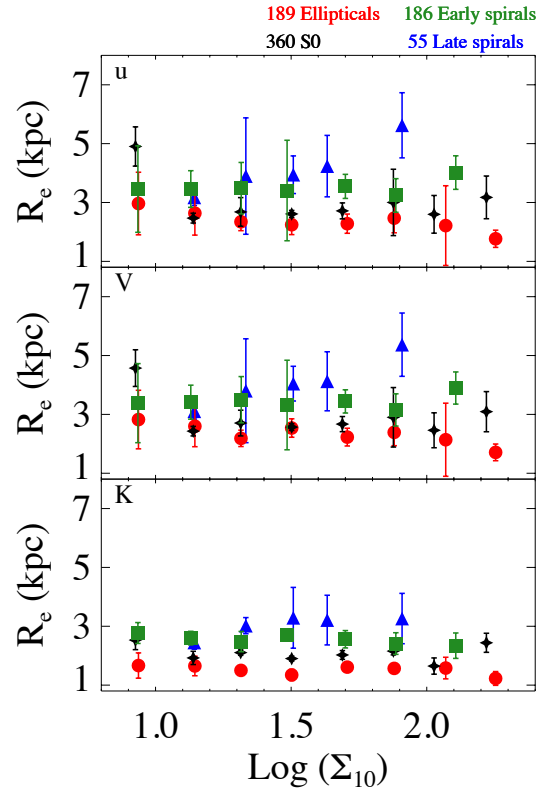
Fig. 12. Weighted median values of R_e in *u*-, *V*-, and *K*-band as a function of the projected local density of the clusters. We divide the *x*-axis into projected local density bins of $0.2 \times \log(\Sigma_{10})$. The colour coding and description are the same as in Fig. 9. We note that the number of galaxies per bin is not constant (see Table 4).

Table 4. Statistical values per bin for each morphological class of galaxies shown inside the Figs. 11 and 12.

| Morphological class	Minimum	Maximum	Mean
Ellipticals	4	46	24
S0s	3	103	45
Early-type spirals	0	60	23
Late-type spirals	0	18	7

Notes. In this table we report the minimum, the maximum, and the mean number of galaxies used for calculating the values of Sérsic index and R_e in the bins of Figs. 11 and 12. Each morphological class is reported separately.

galaxies in order to contrast their morphological properties with the cluster-member galaxies. With this comparison, we can study galaxies evolving inside the gravitation potential of a cluster and galaxies that are located in the "field".

In Fig. 13 we present the weighted median values of Sérsic index as a function of wavelength from optical to NIR for the cluster-member and non-member galaxy samples. We remind the reader that the cluster-galaxy sample differs from the sample used in the previous plots (see Sect. 3.4 for more details). In general, the median *n* of all galaxy types, at all wavelengths, that exist in clusters is larger compared with galaxies located in the field. As we saw in Fig. 3, ellipticals and S0s show a trend of increasing *n* as a function of stellar mass. Therefore, ellipticals and S0s included in this secondary sample have higher average *n* (and R_e) compared to the initial sample because this sample contains brighter (therefore more massive) galaxies.
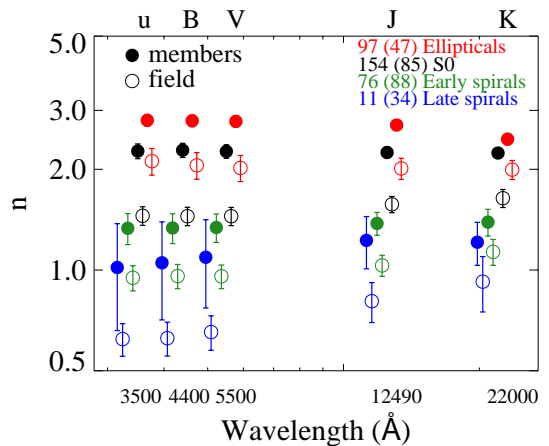
Fig. 13. Median *n* as a function of wavelength for cluster-member and non-member galaxies. Asterisks indicate the cluster sample while filled crosses show the non-member sample. The colour coding and description are the same as in Fig. 6.

Non-member elliptical galaxies show the same trend with cluster ellipticals, namely that *n* remains constant as we move from optical to NIR (the slopes of the least square fit of cluster and non-member ellipticals are both negative and extremely low (~10^{-5}). Here we can see that S0 galaxies present different trends. The Sérsic index of cluster S0s tends to decrease from the optical to the NIR (very low, positive least square slope) while the median *n* values of non-member S0s increases slightly with wavelength (very low, negative least square slope).

Table 5. The percentage changes of n and Re as shown in Figs. 13 and 15.

Morphological class	$(R_e(K)/R_e(u) - 1) \times 100$ cluster galaxies	$(R_e(K)/R_e(u) - 1) \times 100$ non-member galaxies	$(n(K)/n(u) - 1) \times 100$ cluster galaxies	$(n(K)/n(u) - 1) \times 100$ non-member galaxies
Ellipticals	-44 ± 6	-31 ± 13	-12 ± 5	-6 ± 10
S0s	-35 ± 9	-25 ± 8	-1 ± 6	13 ± 10
Early-type spirals	-30 ± 21	-27 ± 5	4 ± 15	20 ± 15
Late-type spirals	-40 ± 30	-27 ± 8	19 ± 45	49 ± 33

Notes. The percentage changes of n and R_e from u- to K-band for cluster and non-member galaxies as presented in Figs. 13 and 15 (see Sect. 4.4.1 for more details of the formulas we used to calculate the percentage changes and their errors).

Spiral galaxies (both cluster and non-member galaxies) tend to increase their median n values as a function of wavelength (positive least square slopes) but within the errors. In general, we performed KS tests among all bands, comparing two different bands each time; we found that the Sérsic index KS test probabilities are > 0.05 for all morphological types. We conclude that the Sérsic index remains constant as a function of wavelength. In Table 5 we present the percentage change of n and R_e and from u- to K-band for cluster and non-member galaxies as presented in Figs. 13 and 15. The percentage changes are calculated from the points (weighted median values, binned data) of Figs. 13 and 15. For example, the percentage R_e change of ellipticals (44%) is calculated from the 100% difference between the points in Fig. 15 using the formula

$$100 \frac{median(R_{e,K}) - median(R_{e,u})}{median(R_{e,u})}. \tag{4}$$

The equivalent R_e change error (± 6%) is calculated with the error propagation theory formula, which is equal to

$$100 \frac{1}{|median(R_{e,u})|} \sqrt{\sigma(R_{e,K})^2 + (\frac{\sigma(R_{e,u})}{R_{e,u}} R_{e,K})^2}. \tag{5}$$

Figures 6 (top panel) and 13 illustrated how the weighted median n changes across different wavelengths. The sample of Fig. 6 contains the 790 cluster galaxies while Fig. 13 presents the sample of cluster galaxies with the non-member galaxies that have $M_V < -19.27$ mag. Following Vulcani et al. (2014), we explored the variation of n using the $\mathcal{N}_Y^X = n(X)/n(Y)$ parameter, where $n(X)$ and $n(Y)$ are the Sérsic index in X- and Y-band, respectively. Measuring the ratio of the Sérsic index of different bands is a way to investigate the stellar populations and spatial structure of galaxies at different wavelengths. These ratios provide a simple but powerful parametrization of galaxy colour gradients (Vulcani et al. 2014; Kennedy et al. 2015). Young and intermediate stars radiate mostly in the optical spectrum while older stellar populations emit in NIR. As a result, galaxies display a different structure due to the inherent distribution of different stellar populations and dust extinction inside the galaxies. Our multi-wavelength analysis provides a very good opportunity to compare values in different wavelengths due to the fact that the images are developed in a homogeneous process rather than fitting galaxies independently in each band.

In Fig. 14 we use the B-band as the reference band and we calculate the $\mathcal{N}$ of each band. We notice that cluster ellipticals have median $\mathcal{N}$ values less than 1 in the K-band while non-member ellipticals have median $\mathcal{N}$ values close to 1 in all bands. Cluster lenticular galaxies do not greatly change the $\mathcal{N}$. Both cluster and non-member spiral galaxies exhibit the same trend with increasing $\mathcal{N}$ values as the wavelength increases. Finally,
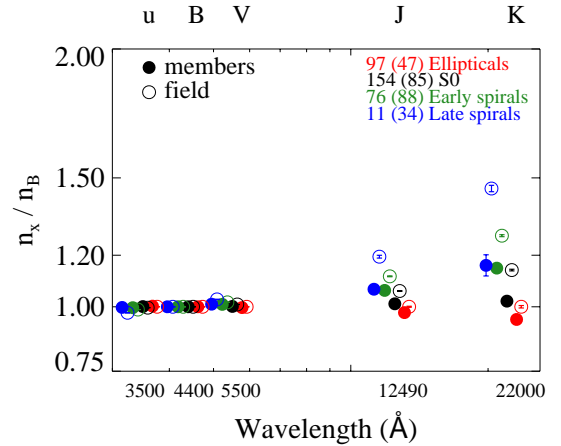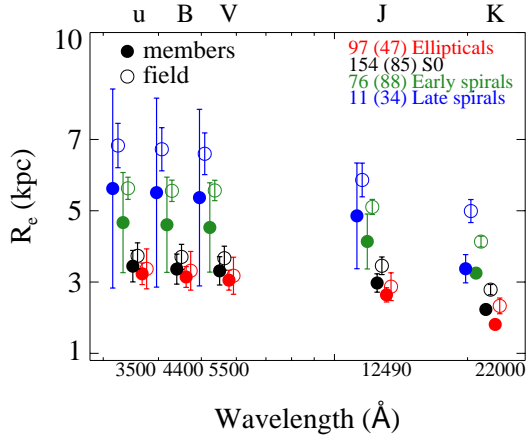

Fig. 14. $\mathcal{N}$ for cluster member and non-member galaxies of different morphological types from optical to NIR. Asterisks indicate the median values of each band of member galaxies while filled crosses are the non-member galaxies. The colour coding and description are the same with Fig. 6.

non-member spirals show greater variation compared to cluster members. We investigate the influence of stellar mass in Fig. 14 by applying stellar mass cuts of $\log_{10}(M_\star) = [9,10,11]$ in both cluster and non-member samples. However, no changes in the variation of $\mathcal{N}$ for ellipticals and S0s, except for those with very high values of stellar mass ($\log_{10}(M_\star) > 11$), are visible.

4.4.2. Effective radius, R_e

Figure 15 presents the median values of R_e as a function of wavelength from optical to NIR for the same sample of cluster members and non-member galaxies. We observe that non-member galaxies display larger R_e compared to the member sample for all morphological types in all bands. Moreover, R_e decreases from optical to NIR in a similar way for all galaxy types (see Table 5 for tabulated values). The general conclusion of Fig. 15 is that ellipticals have smaller R_e than S0s, and S0s have smaller R_e than early-type spirals. Cluster-member galaxies display lower R_e compared to galaxies in the field. This statement holds only for S0s, early-type spirals, and late-type spirals. Ellipticals do not change their R_e for different environments. We applied a K–S test for each morphological class. For ellipticals we found that the KS p-statistic is equal to 0.70 and the D value is 0.40. For the remaining morphological classes, the p-statistics are less that 0.04 and the D values are above 0.80. These results do not change if we include galaxies with higher stellar masses. In contrast to the Sérsic index, we performed KS tests among all bands, comparing two different bands each time and found that the R_e KS test probabilities are < 0.05 for all morphological types of

Fig. 15. Median R_e as a function of wavelength for cluster members and non-member galaxies. Asterisks indicate the cluster galaxies while filled crosses show the non-member galaxies. The colour coding and description are the same as in Fig. 13.
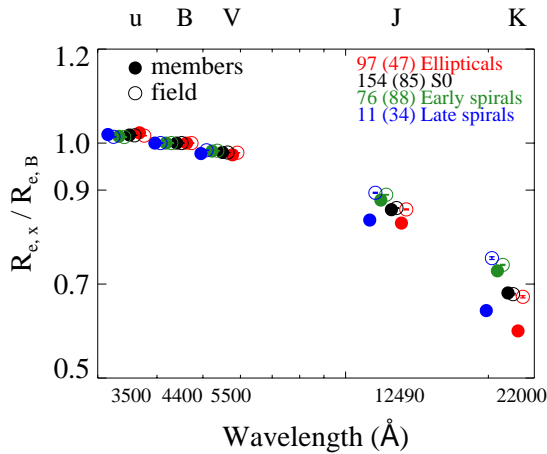
Fig. 16. $\mathcal{R}$ for cluster members and non-member galaxies of different morphological types from optical to NIR. The colour coding and description are the same with Fig. 14.

galaxies (both cluster and non-member galaxies). We conclude that the R_e decreases from u to K-band.

Figure 16 shows the equivalent diagram to Fig. 14 for R_e. The median $\mathcal{R}$ of all morphological types of galaxies, both cluster members and non-members, is smaller in the NIR. In general, $\mathcal{R}$ has values close to 0.7 in the NIR for all galaxies and the largest difference of $\mathcal{R}$ between member and non-member galaxies appears in the K-band but only for ellipticals and late-spirals. Ellipticals, especially those in clusters, tend to have the largest variation from optical to NIR. Lenticulars and early-type spirals present nearly identical median values both inside clusters and in the field in all wavelengths. Non-member late-type spirals (blue crosses) present the lower variation of $\mathcal{R}$ values while the corresponding cluster members (blue asterisks) have larger $\mathcal{R}$ variation than early-type spirals and lenticulars in clusters. We investigate the influence of stellar mass in Fig. 16 following the same approach as in Fig. 14. We applied stellar mass cuts of $\log_{10}(M_\star) = [9,10,11]$ upon the cluster-member and non-member samples and we find no statistically significant correlation. In other words, the R_e decreases with increasing wavelength independent of the stellar mass. The only visible difference is the higher value of $\mathcal{R}$ in field galaxies compared to cluster members for late-type systems. However, given the small number

of late-type galaxies, this should be examined again with larger samples.

5. Discussion

In the previous sections we present the multi-wavelength dependence of the morphological structure of cluster galaxies and compare them with non-member galaxies. In the following paragraphs, we compare our findings with previous studies in more detail.

La Barbera et al. (2010) studied a sample of bright early-type galaxies ($M_r < -20$ mag) based on multi-wavelength (from g- to K-band) imaging. They extracted the structural parameters for each band independently and found that the n remains nearly constant with a large scatter (slight increase from optical to NIR) while the R_e decreases up to 35% from g- to K-band. Our non-member S0s display a slight increase in the Sérsic index (13%) while the n of non-member ellipticals remains the same in the optical bands and decreases slightly in the K-band. Regarding R_e, we also find a decrease as a function of wavelength of ~31% for non-member ellipticals and up to 25% for non-member S0s.

Kelvin et al. (2012) studied the optical and NIR morphology of galaxies in the local Universe extracted from the GAMA survey. These latter authors fitted single-Sérsic functions in all bands (from u to K) independently in a magnitude-limited sample ($r \leq 19.4$). For early-type galaxies, Kelvin et al. (2012) find that R_e decreases by up to 38% while we find a decrease of $31\% \pm 13$ ($25\% \pm 8$) in R_e for non-member ellipticals (S0s) which is a statistically consistent result. In addition, Kelvin et al. (2012) find that the Sérsic index of early-type galaxies increases by ~52% while we find that the Sérsic index of non-member ellipticals (S0s) remains constant with wavelength: $-6\% \pm 10$ ($13\% \pm 10$). As for late-type galaxies, they found that the R_e decreases up to 25% from g- to K-band and the Sérsic index increases by ~52%. In our work, the R_e decreases by 27 ± 5 (27 ± 8) for non-member early spirals (late spirals), a statistically consistent result, while the Sérsic index increases for non-member spiral galaxies ($20\% \pm 15$ and $49\% \pm 33$ for early- and late- type spirals, respectively). Vulcani et al. (2014) applied the same methodology as that of our study to galaxies with $M_r < -21.2$ and $z < 0.3$ derived from the GAMA survey. These latter authors found that the R_e of early-type galaxies decreases by up to 45%, which is larger than our result. On the other hand, Vulcani et al. (2014) find that the Sérsic index of early-type galaxies remains nearly constant as a function of wavelength which is statistically consistent with our result. However, the R_e of late-type systems decreases up to 25% from u- to H-band (similar to our result) and the Sérsic index increases up to 38% which is close enough to our work.

Kennedy et al. (2015) studied the wavelength dependence of galaxy structure, using the parameters derived by Vulcani et al. (2014) and focusing on a more local sample ($z < 0.15$). Kennedy et al. (2015) found that the n and R_e of the early-type galaxies with $M_r \sim -20$ decrease (12% and 23% respectively) from g- to H-band. As these latter authors examine brighter galaxies samples ($M_r \sim -21$ and $M_r \sim -22$), the n of early types slightly increases (5%) and the R_e decreases (25%–33%). Moreover, for $M_r \sim -20$, the n of late-type galaxies increases (up to 29%) while their R_e decreases by up to 13%. The R_e of late-type galaxies displays a similar behaviour with the less bright galaxies (decrease from 15% to 12% as a function of wavelength) while the n increases from 40 to 55%.

We summarise the literature results as follows: In field galaxies, there is a clear trend with increasing wavelength. Their size becomes smaller for all galaxy types, while the Sérsic index increases for late-type galaxies and remains near constant with small variations for the early-type galaxies depending on the details of the sample selection. We note that all previous studies with which we can compare our results have focused on field galaxies and use different proxies in order to define morphology; for example colour and n cuts or visual morphology. There are, however, very significant difficulties to be considered when comparing different studies. The details governing the sample selection (galaxy mass and morphology) and the exact definition of the environment are important. We should keep in mind that subtle differences make direct comparisons challenging and may be responsible for the discrepancies found in different studies.

In our study, we examine two subsets of cluster galaxies. The first one includes all cluster galaxies of the nine clusters (see Figs. 5–12) and the second one includes the cluster galaxies that have $M_V < -19.27$ (see Figs. 13–16). With the first cluster subsample, we study the structure parameters and the influence of cluster environment. The second cluster subsample (bright cluster galaxies) is used in order to compare the values of n and R_e with the non-member sample and facilitate the comparison of the results of this study with previous findings.

The Sérsic index of all classes of the first subset of cluster galaxies remains the same as a function of wavelength (optical to NIR). The R_e decreases as a function of wavelength. The local projected density (even less the R_{BCG}) might affect the observed n of cluster member galaxies (S0s and spirals) but not the variation of n with wavelength. The local projected density and the R_{BCG} do not affect the R_e.

The stellar mass plays an important role in the values of structural parameters (as we show in Figs. 3 and 4). More massive galaxies tend to have greater values of Sérsic index and R_e. The effect is obvious when we compare the first subset of cluster member galaxies in Figs. 6 and 8 with the second subset of cluster member galaxies (shown in the asterisks) in Figs. 13 and 15. However, we clearly see that the structural variation with wavelength is statistically the same for each galaxy type as that in clusters independent of luminosity (and stellar mass) as also shown in Kennedy et al. (2015).

We do not observe any clear trend in structural parameters with projected local density (Figs. 11 and 12). Although small trends exist, such as an increase of the median n for late-type galaxies and a decrease of the median R_e for early-type spirals up to $\log(\Sigma_{10}) \sim 1.5$, the scatter of these measurements is high. Two reasons could be responsible for the lack of clear trends. Firstly, all galaxies of our cluster member sample are inside $0.64 \times R_{BCG}$, so they are not far away from the cluster centre. An updated analysis of cluster galaxies located in the periphery of clusters (outside $0.64 \times R_{BCG}$) could shed more light on the effect of cluster gravitational potential to the structure of its galaxies. Secondly, the sample of our nine galaxy clusters is not homogenous in terms of membership and dynamical relaxation. Some clusters have more than 100 members, others have only 30, and only seven of the nine have signs of substructures.

Our analysis of the effects of cluster environment (R_{BCG} and Σ_{10}) upon the structure reveal that the n and R_e of ellipticals and S0s are statistically constant across the R_{BCG} and the local projected density (Σ_{10}). As for late spirals, we find minimum values of n and maximum values of R_e at the position of $0.3-0.4 \times R_{BCG}$. Early spirals have hints for maximum R_e values in those regions. The study of Ramella et al. (2007) showed that seven out of nine galaxy clusters have substructures. We already know that

processes like preprocessing and minor merger events are frequent near substructures, influencing the evolution of galaxies. Six out of fourteen substructures of the seven galaxy clusters are located near $0.3-0.4 \times R_{BCG}$. Even if the number of late spirals is low, it is possible that the minimum and maximum values of n at these positions are hints for interesting results about structure parameters near the substructure positions. Including more galaxy clusters in an updated study we lead to an improved statistical analysis are therefore more robust conclusions.

In the last part of our analysis, we study the bright cluster galaxies (second sample), comparing them with the non-member galaxies. Park et al. (2007) and Davies et. al. (in prep.) found that at fixed morphology and luminosity, other physical properties of local galaxies, such as colour, colour gradient, concentration, size, velocity dispersion, star formation rate, and dust content, are nearly independent of local density. Likewise, Kelkar et al. (2015), found no significant difference in the size distribution of cluster and field galaxies of a given morphology. In this study we find that at fixed morphological bins, bright cluster galaxies show different trends compared to the non-member galaxies.

Bright cluster galaxies have larger Sérsic index and smaller R_e than their non-member counterparts (see Figs. 13 and 15). This might imply that bright cluster galaxies have more concentrated light profiles compared to non-member galaxies. In particular, an increase in the Sérsic index for spiral galaxies (early and late type) and S0s could be due to the process of adding mass in the central parts of galaxies (gas or stars). Tidal interactions (galaxy-galaxy or galaxy-cluster potential) and/or harassment are known to have these effects.

The variation of Sérsic index with wavelength is effectively absent for cluster member galaxies in comparison with the variations of non-member galaxies (also in comparison with Vulcani et al. (2014). The absence of Sérsic index variation in bright cluster galaxies and the fact that bright cluster galaxies appear more concentrated (higher Sérsic indices) compared to non-member counterparts lead us to the following. If we assume that galaxies located in the field are attracted by the cluster potential and pass by the inner part of the clusters, the effect of environment could change their light distribution. In particular, material begins to move to the centre of the galaxies (Byrd & Valtonen 1990) and the light profiles become more dominant (increase of Sérsic index in optical and NIR wavelengths) than the light profiles of non-member counterparts. At the same time this increase of Sérsic index should not happen in the same way both in optical and NIR, so we can have a decrease of $\mathcal{N}$ as the galaxy moves from the field into the cluster. In addition, another possible scenario is the following: merging of (smaller) galaxies falling into the clusters interact or merge with cluster members, increasing their nuclear stellar bulge.

Regarding size as a function of wavelength, cluster galaxies appear to show little variation compared to the non-member galaxies. Ellipticals and late-type spiral cluster galaxies are the only exception; these have slightly smaller $\mathcal{R}$ compared to non-member galaxies. These results show that elliptical galaxies in clusters have the same $\mathcal{N}$ change as in the field but at the same time have smaller $\mathcal{R}$ values. This means that the physical process that forces evolution in cluster galaxies changes their size in a different way in optical than in NIR while at the same time their light concentration changes in the same way, always compared to the non-member galaxies. In case of early-type spirals and S0s we see the opposite trend. Bright S0s and early spirals in clusters follow exactly the same size change as a function of wavelength as the non-member equivalent populations (see Fig. 15). At the same time these galaxies show an $\mathcal{N}$ slightly higher than

1 in the IR region which is a much lower value than what is observed in the our non-member galaxies and also in other studies. These results are an indication that different morphological types can be affected in a different way by the environment. It remains challenging to assess which processes are responsible for the structural differences between each morphological type of cluster galaxies.

We already know that there is a weak connection between the different evolutionary mechanisms in clusters and the distance from the $R_{\rm BCG}$ (Boselli & Gavazzi 2006). Inside the virial radius and close to the centre of galaxy clusters (where the density, the temperature of the intergalactic medium (IGM), and the velocity of galaxies have high values), tidal interactions could affect the morphology of galaxies and consequently their light profiles. Galaxy–galaxy interactions, even if they take place near the centre of rich clusters, remain fairly rare ($t_{\rm enc} \sim 10^8\,yr$) and the relative velocities of the encounters are high compared to their typical rotational speeds. The most efficient processes close to the centre of a cluster are the galaxy–cluster IGM interactions, harassment, and ram-pressure. Our findings support the idea that the above processes apply to cluster galaxies (spirals and S0s) if we compare the n and $R_{\rm e}$ with their non-member counterparts.

An upcoming study on the OMEGACAM data (largee FoV 1 $\sim$ degree) will increase the number of WINGS galaxies and will shed more light on the difference between local cluster galaxies and the interpretation of the physical mechanisms that affect the evolution of galaxies in the peripheral regions.

6. Conclusions

In this paper we study the structural parameters of cluster galaxies across optical and NIR wavelengths. The structural parameters have been calculated with the state-of -the-art software GALAPAGOS-2 which uses single-Sérsic functions (from u- to K-band).

Our multi-wavelength analysis of nine galaxy clusters leads us to the following conclusions.

1. The weighted median value of Sérsic index of cluster member galaxies remains constant across optical and NIR wavelengths (see upper panel of Fig. 6) while the median values of $R_{\rm e}$ tend to decrease for all morphological types (see upper panel of Fig. 8).
2. Late-type spiral galaxies in the inner regions of the clusters and in the higher-density regions show a slight increase in the average Sérsic index compared to the outer and lower-density regions of the clusters, respectively. Sérsic index of lenticular and early-type spiral galaxies seems to be affected only by the environment density. Lenticular galaxies increase their average Sérsic index in the higher-density environment, like late-type spirals do, while early-type spiral galaxies show the opposite trend (see middle and down panels of Fig. 6).
3. Late-type spiral galaxies appear to have smaller average $R_{\rm e}$ when they are at the outer area of the cluster, even though the difference is within the error bars. The median $R_{\rm e}$ is larger in higher local densities than in regions with lower local densities. In contrast, the size of ellipticals, S0s, and early-type spirals does not change noticeably as a function of the environment (see middle and down panels of Fig. 8).
4. Late-type spirals display a decrease in their median Sérsic index as a function of the distance from the cluster centre up to $\sim 0.3 \times R_{\rm BCG}$ in the optical bands, while further out n remains statistically constant (see Fig. 9). Early-type spirals have constant $R_{\rm e}$ values across $R_{\rm BCG}$ while late-type spirals

increase their median $R_{\rm e}$ up to $\sim 0.35 \times R_{\rm BCG}$ in optical and especially in NIR bands (see Fig. 10).
5. We do not observe any clear trend of structural parameters with projected loca l density (see Figs. 11 and 12).
6. Early- and late-type spirals, as well as S0s, which are cluster members fulfilling the $M_{\rm V} = -19.27$ mag selection limit, display on average greater Sérsic index (see Fig. 13) and smaller $R_{\rm e}$ than their non-member counterparts (see Fig. 15). This is not the case for ellipticals.
7. Despite the apparent trends seen in Figs. 13 and 15, no statistically significant changes are observed in the variation of the Sérsic index and $R_{\rm e}$ for any galaxy type fulfilling the $M_{\rm V} = -19.27$ mag selection limit, as a function of wavelength.

References

Bamford, S. P., Häußler, B., Rojas, A., Vika, M., & Cresswell, J. 2012, IAU Symp., 284, 301
Barden, M., Häußler, B., Peng, C. Y., McIntosh, D. H., & Guo, Y. 2012, MNRAS, 422, 449
Bekki, K. 1998, ApJ, 502, L133
Bell, E. F., McIntosh, D. H., Katz, N., & Weinberg, M. D. 2003, ApJS, 149, 289
Berriman, G. B., Good, J. C., Laity, A. C., & Kong, M. 2008, ASP Conf. Ser., 394, 83
Bertin, E. 2011, ASP Conf. Ser., 442, 435
Bertin, E., & Arnouts, S. 1996, A&AS, 117, 393
Boselli, A., & Gavazzi, G. 2006, PASP, 118, 517
Butcher, H., & Oemler, Jr., A. 1978, ApJ, 219, 18
Byrd, G., & Valtonen, M. 1990, ApJ, 350, 89
Calvi, R., Poggianti, B. M., Vulcani, B., & Fasano, G. 2013, MNRAS, 432, 3141
Cava, A., Bettoni, D., Poggianti, B. M., et al. 2009, A&A, 495, 707
Cerulo, P., Couch, W. J., Lidman, C., et al. 2017, MNRAS, 472, 254
Desai, V., Dalcanton, J. J., Aragón-Salamanca, A., et al. 2007, ApJ, 660, 1151
D'Onofrio, M., Bindoni, D., Fasano, G., et al. 2014, A&A, 572, A87
Dressler, A. 1980, ApJS, 42, 565
Dressler, A., Oemler, Jr., A., Couch, W. J., et al. 1997, ApJ, 490, 577
Driver, S. P., Norberg, P., Baldry, I. K., et al. 2009, Geophys., 50, 12
Fasano, G., Poggianti, B. M., Couch, W. J., et al. 2000, ApJ, 542, 673
Fasano, G., Marmo, C., Varela, J., et al. 2006, A&A, 445, 805
Fasano, G., Vanzella, E., Dressler, A., et al. 2012, MNRAS, 420, 926
Fasano, G., Poggianti, B. M., Bettoni, D., et al. 2015, MNRAS, 449, 3927
Fritz, J., Poggianti, B. M., Bettoni, D., et al. 2007, A&A, 470, 137
Fritz, J., Poggianti, B. M., Cava, A., et al. 2011, A&A, 526, A45
Fritz, J., Poggianti, B. M., Cava, A., et al. 2014, A&A, 566, A32
Gunn, J. E., & Gott, III., J. R. 1972, ApJ, 176, 1
Häußler, B., Bamford, S. P., Vika, M., et al. 2013, MNRAS, 430, 330
Häussler, B., McIntosh, D. H., Barden, M., et al. 2007, ApJS, 172, 615
Hubble, E., & Humason, M. L. 1931, ApJ, 74, 43
Icke, V. 1985, A&A, 144, 115
Kelkar, K., Aragón-Salamanca, A., Gray, M. E., et al. 2015, MNRAS, 450, 1246
Kelvin, L. S., Driver, S. P., Robotham, A. S. G., et al. 2012, MNRAS, 421, 1007
Kennedy, R., Bamford, S. P., Baldry, I., et al. 2015, MNRAS, 454, 806
Kim, D., & Im, M. 2013, ApJ, 766, 109
La Barbera, F., de Carvalho, R. R., de La Rosa, I. G., et al. 2010, MNRAS, 408, 1313
Larson, R. B., Tinsley, B. M., & Caldwell, C. N. 1980, ApJ, 237, 692
Lubin, L. M., Oke, J. B., & Postman, M. 2002, AJ, 124, 1905
MacArthur, L. A., Courteau, S., Bell, E., & Holtzman, J. A. 2004, ApJS, 152, 175
Moore, B., Katz, N., Lake, G., Dressler, A., & Oemler, A. 1996, Nature, 379, 613
Moore, B., Lake, G., & Katz, N. 1998, ApJ, 495, 139
Moore, B., Lake, G., Quinn, T., & Stadel, J. 1999, MNRAS, 304, 465

Moretti, A., Gullieuszik, M., Poggianti, B., et al. 2017, A&A, 599, A81
Moretti, A., Poggianti, B. M., Fasano, G., et al. 2014, A&A, 564, A138
Omizzolo, A., Fasano, G., Reverte Paya, D., et al. 2014, A&A, 561, A111
Park, C., Choi, Y.-Y., Vogeley, M. S., et al. 2007, ApJ, 658, 898
Peng, C. Y., Ho, L. C., Impey, C. D., & Rix, H.-W. 2002, AJ, 124, 266
Pignatelli, E., Fasano, G., & Cassata, P. 2006, A&A, 446, 373
Poggianti, B. M., Fasano, G., Bettoni, D., et al. 2009, ApJ, 697, L137
Postman, M., Franx, M., Cross, N. J. G., et al. 2005, ApJ, 623, 721
Ramella, M., Biviano, A., Pisani, A., et al. 2007, A&A, 470, 39
Robotham, A. S. G., Norberg, P., Driver, S. P., et al. 2011, MNRAS, 416, 2640
Schmidt, K.-H., Bohm, P., & Elsasser, H. 1997, Astron. Nachr., 318, 81
Sersic, J. L., Pastoriza, M. G., & Carranza, G. J. 1968, Astrophys. Lett., 2, 45
Smail, I., Dressler, A., Couch, W. J., et al. 1997, ApJS, 110, 213
Valentinuzzi, T., Woods, D., Fasano, G., et al. 2009, A&A, 501, 851
van Dokkum, P. G., Franx, M., Fabricant, D., Illingworth, G. D., & Kelson, D. D. 2000, ApJ, 541, 95
Varela, J., D'Onofrio, M., Marmo, C., et al. 2009, A&A, 497, 667
Vika, M., Bamford, S. P., Häußler, B., et al. 2013, MNRAS, 435, 623
Vika, M., Bamford, S. P., Häußler, B., & Rojas, A. L. 2014, MNRAS, 444, 3603
Vika, M., Vulcani, B., Bamford, S. P., Häußler, B., & Rojas, A. L. 2015, A&A, 577, A97
Vulcani, B., Poggianti, B. M., Aragón-Salamanca, A., et al. 2011a, MNRAS, 412, 246
Vulcani, B., Poggianti, B. M., Dressler, A., et al. 2011b, MNRAS, 413, 921
Vulcani, B., Poggianti, B. M., Fasano, G., et al. 2012, MNRAS, 420, 1481
Vulcani, B., Poggianti, B. M., Oemler, A., et al. 2013, A&A, 550, A58
Vulcani, B., Bamford, S. P., Häußler, B., et al. 2014, MNRAS, 441, 1340
Whitmore, B. C., Gilmore, D. M., & Jones, C. 1993, ApJ, 407, 489

Appendix A: Comparison of GALAPAGOS-2 with GASPHOT

D'Onofrio et al. (2014) applied the software called GAlaxy Surface PHOTometry (GASPHOT; Pignatelli et al. 2006), on *B*-, *V*- and *K*-band images of WINGS galaxies. Here we compare the structural parameters of GALAPAGOS-2 with GASPHOT. Fig. A.1 shows the magnitude, *n* and R_e of the cross-matched cluster galaxies in *V*-band.

GASPHOT and GALFITM measure the same magnitudes for all galaxy types. GASPHOT measures smaller sizes for small elliptical galaxies. In addition, we see that for galaxies with *n* > 2, GASPHOT measures larger light profiles compared to GALFITM. The above discrepancy could be due to various effects (Pignatelli et al. 2006; Häussler et al. 2007). The most important is GASPHOT uses the 1D approach while GALFITM uses a 2D method. Secondly, the sky has been measured in two different ways, which can lead to substantial differences in the fit parameters (Häussler et al. 2007). Finally, we must not forget that average uncertainties of the structural parameters apply to both software packages as D'Onofrio et al. (2014) showed. The uncertainty range for R_e is from 7% to 20% while for *n* this is from 20% to 30%. In addition, D'Onofrio et al. (2014) showed these two methods to have differing sensitivity to the peculiar features of galaxies and that they behave differently in weighting the various (inner and outer) galaxy regions.
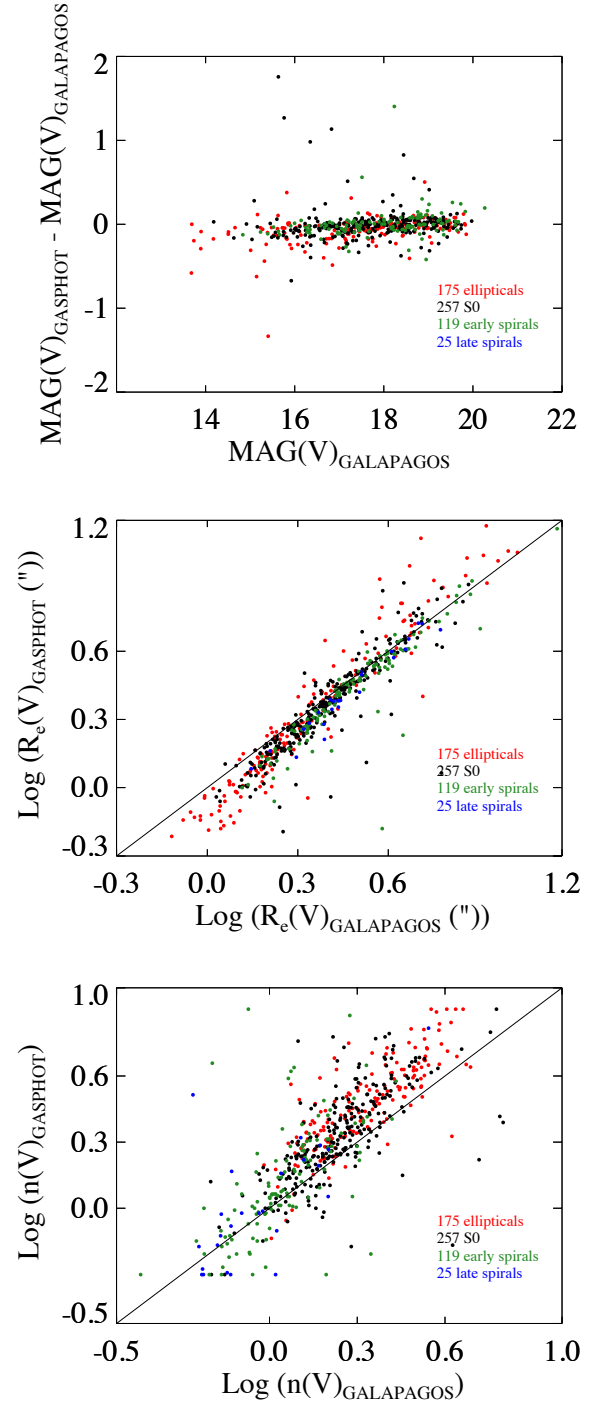

Fig. A.1. Structural parameters for all galaxies in *V*-band.